

# GRID-CONNECTED PHOTOVOLTAIC SYSTEMS WITH MULTILEVEL CONVERTERS – MODELING AND ANALYSIS

MIHĂIȚĂ-ALEXANDRU ILIE<sup>1</sup>, DAN FLORICĂU<sup>1</sup>

**Keywords:** Grid-connected; Photovoltaic system; Three-level active neutral point clamped; Optimal control; Three-level dc-dc boost converter.

**In this paper, a comparison between three double-stage grid-connection systems in central inverter configuration is presented. This configuration can be used to obtain a wide power range and is suitable for the connection to three-phase grids. In this case, the photovoltaic (PV) panels are connected to the inverter via a dc-dc converter to ensure an optimal dc voltage level. The focus is on the characteristics and properties of the used converter’s structures. All the design steps of a grid connection system are also presented. Both two-level (2L) and three-level (3L) voltage structures are implemented. At the end of the paper, a detailed analysis highlights the advantages and disadvantages of the three photovoltaic systems connected to the grid.**

## 1. INTRODUCTION

Electricity demand has been growing nowadays and is forecast to continue to grow in the future. Renewable energy sources based on sunlight have also received significant attention in recent years. Numerous studies have been presented in the literature on systems allowing grid integration of PV arrays [1–5]. The way in which solar panel arrays can be configured depends on the level of power being installed. In [6] a classification is made. The most popular dc-ac conversion structure for central inverter configuration is 2L-VSC (2 level – voltage source converter). The installed power can exceed 1 MW, as shown in [6]. Also, in this category, multi-level voltage structures can be used, such as 3L-NPC (3 level – neutral point clamped) [7, 8], 3L-ANPC (3 level – active neutral point clamped) [7, 8] etc.

Usually, the PV panel array does not connect directly to the inverter input. Between these two parts, there is a dc-dc converter which is designed to provide a constant dc-link voltage (Fig. 1). In PV systems, these structures are controlled using a maximum power point tracking (MPPT) algorithm. For example, in [9,10] comparative studies between several types of methods are carried out; thus, the characteristics and performances of the presented structures are highlighted.

Another issue that is discussed with maximum attention in PV systems is synchronizing the conversion chain to the grid. In [1, 11–12], several ways of grid synchronization are presented that can be used both for PV applications and for other types of renewable energy sources. The most important part is to determine the phase of the fundamental harmonic of the grid voltage. The common way to determine this parameter is to implement a phase detector called PLL (phase-locked loop). Some basic examples have been presented in [13], and later more complex structures have been introduced to better cope with limiting situations such as harmonic content, phase jump, operation under unbalanced or fault conditions, etc. The most popular structures of this type are the following: DSOGI (dual second-order generalized integrator) [14] or DDSRF (decoupled double synchronous reference frame-PLL) [15].

The objective of this paper is to show the implementation and configuration of three PV array grid integration systems.

This is structured as follows. Section 2 presents the overall structure of a grid-connected system. In the next section, three grid connection systems using two and three voltage level conversion structures are presented. In each subsection, the most important features of the structures used are highlighted, as well as some computational relationships used in the design. The results and their analysis are presented in section 4; the focus has been put on the performances obtained at the system output and on the main differences between the three cases considered. Finally, section 5 is dedicated to the most important conclusions.

## 2. PV SYSTEM CONFIGURATION

Figure 1 shows the minimal block diagram of a double-stage system. Also, at the bottom of the figure, the basic control functions of a grid-connected system are mentioned. Synchronization to the grid is based on the monitored voltage at the point of common coupling (PCC). The control part is based both on measured values on different sides of the system and on some externally imposed values.

The dc supply voltage  $V_{DC}$  is set at the design stage. A value must be imposed at which the inverter operates in good conditions ( $V_{DC}^*$ ). Another parameter that can be externally imposed is the maximum power injected. Therefore,  $P_{limit}^*$  will set the maximum level of power injected into the grid.

Since the system is in a double-stage configuration, the limitation  $P_{limit}^*$  can be implemented at the MPPT level.

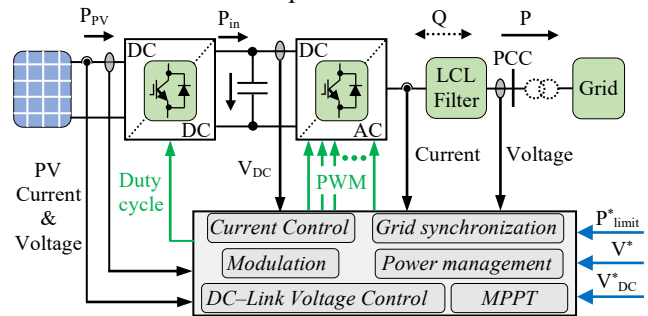


Fig. 1 – Block diagram of the grid-connected PV system.

<sup>1</sup> University Politehnica of Bucharest, Electrical Engineering Faculty, mihaita.ilie@upb.ro, dan.floricau@upb.ro



The LCL filter has the structure shown in Fig. 4. The main conditions based on which the filter parameters are determined are:

- the value of the filter capacity  $C_f$  is limited by the power factor decrease, usually less than 5 % of the base capacity, calculated at rated power.

$$C_f < 5\% \cdot C_b = 5\% \frac{1}{\omega_g \cdot Z_b}; Z_b = \frac{(V \cdot \sqrt{3})^2}{P_{PV}} \quad (7)$$

- the resonant frequency of the filter must be 10 times the mains frequency and less than half the switching frequency used in the dc-ac structure.

$$10 \cdot f_g \leq f_r \leq 0.5 \cdot f_{sw} \quad (8)$$

- the value of the attenuation resistance  $R_d$  should be a maximum of one-third of the impedance of the filter capacitance at the resonant frequency.

$$R_d = \frac{1}{3 \cdot \omega_r \cdot C_f}; \omega_r = \sqrt{\frac{L_i + L_g}{L_i \cdot L_g \cdot C_f}} \quad (9)$$

$L_i$  and  $L_g$  inductance values are determined depending on the type of inverter used, these cases will be detailed later.

Considering all these general aspects, three cases of grid connection systems will be presented.

General parameters, which will be considered the same in all cases studied, are presented in Table 1.

Table 1  
General parameters of systems.

Parameter	Description	Value
$P_{PV}$	Maximum PV power	18.8 kW
$V_{[RMS]}$	Terminal voltage (phase)	230 V
$f_g$	Grid frequency	50 Hz
$V_{DC}$	Dc-link voltage	800 V
$L$	Grid inductance	2.5 mH
$R$	Grid resistance	10 mΩ
$V_{PV}$	PV array voltage	537 V
$I_{PV}$	PV array current	35 A
$V_{DC}^*$	Reference dc-link voltage	800 V
$V_{[RMS]}^*$	Reference terminal voltage	230 V
$f_g^*$	Reference grid frequency	50 Hz

### 3. PV SYSTEMS WITH MULTILEVEL TOPOLOGIES

#### 3.1. CLASSIC PV SYSTEM

The classical PV grid connection system has only two voltage level conversion structures (Fig. 4). These structures are often used because they have a simple structure and provide good performance. Looking at the classical PV system, from source to grid, the first conversion structure is the two-level (2L) dc-dc stage. The

inductance  $L_{b\_1}$  of the dc-dc boost stage structure is calculated with the following relation:

$$L_{b\_1} \geq \frac{V_{PV}}{4 \cdot \Delta i_{L_{b\_1}} \cdot f_{sw\_1}} \quad (10)$$

where,  $\Delta i_{L_{b\_1}}$  represents the maximum value of the current ripple at the output of the inductor  $L_{b1}$ , which was considered 10% of the maximum value of the current injected by the PV array,  $I_{PV}$ , and  $f_{sw\_1}$  is the switching frequency at which the switch S operates.

In this study  $f_{sw\_1} = 20$  kHz. Thus, a value of inductance  $L_{b1} = 1.9$  mH was obtained.

The capacitance in the dc-link was calculated with relation (5), resulting in a value of 4.6 mF. This capacitance must be sufficient to absorb both harmonics from the inverter operation and the dc-dc stage operation.

In this case, the dc-ac topology is the classical 2L-VSC type. This converter has a simple structure and allows the implementation of several control strategies based on the PWM technique. In this paper, the classical PWM control of sinusoidal type has been considered. By means of it, a switching frequency  $f_{sw} = 5$  kHz has been set.

A major drawback of this topology is that the voltage switched by the switches equals the voltage in the dc-link. This leads to a higher price of the devices, a high level of losses, and a limitation of the switching frequency and/or maximum output power.

Because of the harmonics in the voltage waveform at the inverter output, it is necessary to mount a passive filter between the converter and the PCC.

To start the design of the passive filter, considered in this case LCL type, the maximum power of the filter  $P_F = 20$  kW was imposed. In addition, the current ripple value is set to 10% of the value of the current injected into the grid. Therefore, the value of these ripples is determined based on relation (11).

$$\Delta i_{\max} = 10\% \frac{P_F \cdot \sqrt{2}}{3 \cdot V} \quad (11)$$

Considering the configuration of the inverter and the value of current ripples, the inductance on the inverter side is calculated with the relation:

$$L_{i\_1} \geq \frac{V_{DC}}{4 \cdot f_{sw} \cdot \Delta i_{\max}} \quad (12)$$

resulting in an inductance  $L_{i\_1} = 8.3$  mH.

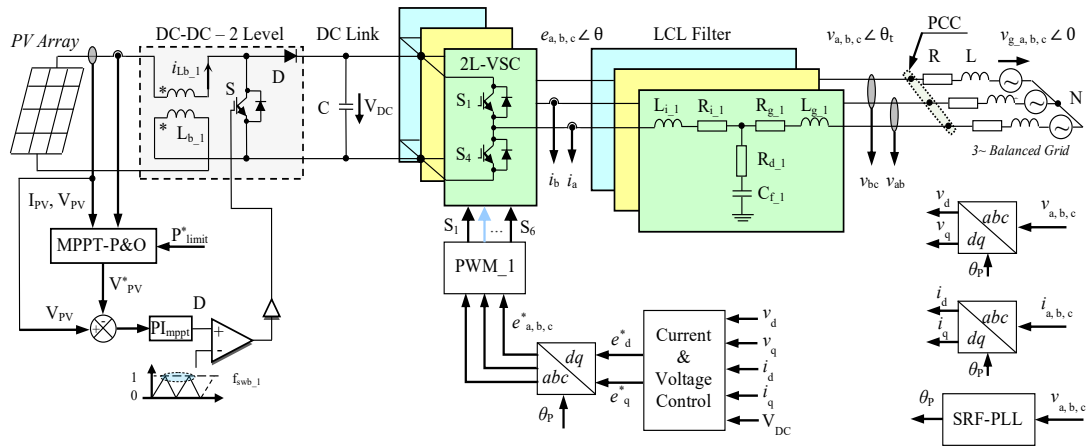


Fig. 4 – Classic PV system based on 2L converters.

The inductance on the grid side must provide good attenuation of harmonics. In [21] it is recommended that this attenuation should be about 20 %, resulting in the ratio of the two filter inductances  $r_1 = L_{g,1} / L_{l,1}$ , so  $L_{g,1} = 1.2$  mH.

According to relation (7), the value of the filtration capacity must be kept below 5 % of the base value. In this case, we first considered 2 % of this basic value, obtaining a capacitance of about 8  $\mu$ F. To respect the above-mentioned conditions, this value was adjusted to 6.5  $\mu$ F, a value that provided a sufficient frequency band for the filter. The attenuation resistance, relation (9), was 4  $\Omega$ , which contributed to better system stability.

In this case, even if the number of switches is smaller, their cost is higher because they support a higher voltage. Also, the inductor values in the 2L dc-dc boost converter structure and the passive LCL filter have significant values, which will lead to a higher cost.

### 3.2. PV SYSTEM WITH 3L CONVERTERS

The second grid connection system consists of conversion structures with three voltage levels (Fig. 5). The hardware component of the system is like the previous case, *i.e.*, the PV array remained in the same configuration, so the same power level is available on the dc side, as well as the parameters modeling the grid. Thus, it was necessary to modify the passive filter on the output side because the harmonic content is different compared to the previous case. Therefore, if there is another filter, the current control side must be reconsidered. The  $PI_{d,2}$  and  $PI_{q,2}$  regulators will be tuned to the new system characteristics.

The structure of the 3L dc-dc boost stage [22] provides an apparent switching frequency at the input inductor terminals ( $L_{b,2}$ ) equal to twice the switching frequency set on the control side. Therefore, to obtain the same effect on the input side, the switching frequency can be reduced by half, *i.e.*,  $f_{sw,2} = 10$  kHz. The inductance value in the 3L boost converter structure was determined with relation (13).

$$L_{b,2} \geq \frac{V_{PV}}{16 \cdot \Delta i_{L_{b,2}} \cdot f_{sw,2}} \quad (13)$$

resulting in an inductance value  $L_{b,2} = 0.95$  mH, about twice as small as in the previous study.

In dc-link, the same equivalent value of the filter capacitance was considered, *i.e.*, 4.6 mF, according to relation (5).

In this second case studied, the dc-ac conversion topology is 3L-NPC. As can be seen in Fig. 5, the structure of this converter is more complex, there are four active switches on each bridge arm as well as two clamp diodes. The two clamp diodes have been added to generate load currents closing paths during times when the output voltage is zero.

Unlike the 2L structure, in this case, the power devices switch only half of the dc supply voltage. The 3L-NPC structure is controlled by the POD – SPWM (phase opposite disposition) [7]. Therefore, in the design stage of the LCL filter, the inductance on the inverter side will have expression (14).

$$L_{i,2} \geq \frac{V_{DC}}{8 \cdot f_{sw} \cdot \Delta i_{max}} \quad (14)$$

resulting in a value of  $L_{i,2} = 4.2$  mH, the values of the maximum current ripple and frequency being equal to those of the previous case.

Thus, the cost of inductors can be reduced, compared to the previous case, because their size is smaller. In addition, an additional saving can be made from the cost of switches, which support a lower voltage level.

Starting from the same value of the filter capacitance as in the previous case, *i.e.*, 8  $\mu$ F, the filter frequency band was adjusted so that the design conditions were met, and a harmonic attenuation of 20 % on the mains side of the filter was obtained. These modifications resulted in a filter capacitance  $C_{f,2} = 5.5$   $\mu$ F, a factor  $r_2 = 0.3$ , so  $L_{g,2} = 1.3$  mH, and an attenuation resistance  $R_{d,2} = 6.5$   $\Omega$ .

### 3.3. PV SYSTEM USING 3L-ANPC INVERTER

In the third case studied, conversion structures with three voltage levels were also considered. The major difference is the dc-ac structure, which is of the 3L-ANPC type (Fig. 6). The dc-dc stage is the same as in the second case study, so its inductance has been calculated above.

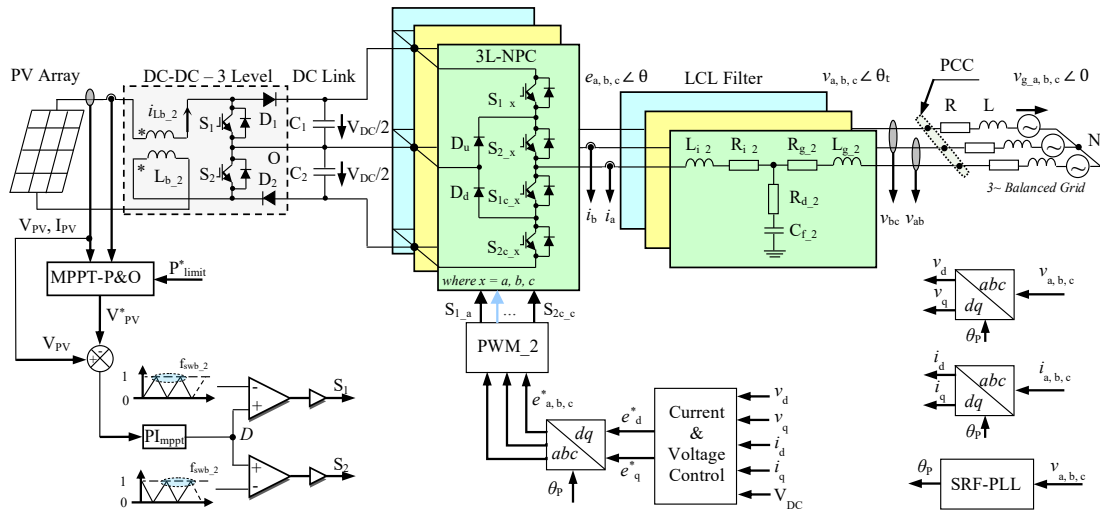


Fig. 5 – Grid-connected system based on 3L-NPC and boost dc-dc 3L.

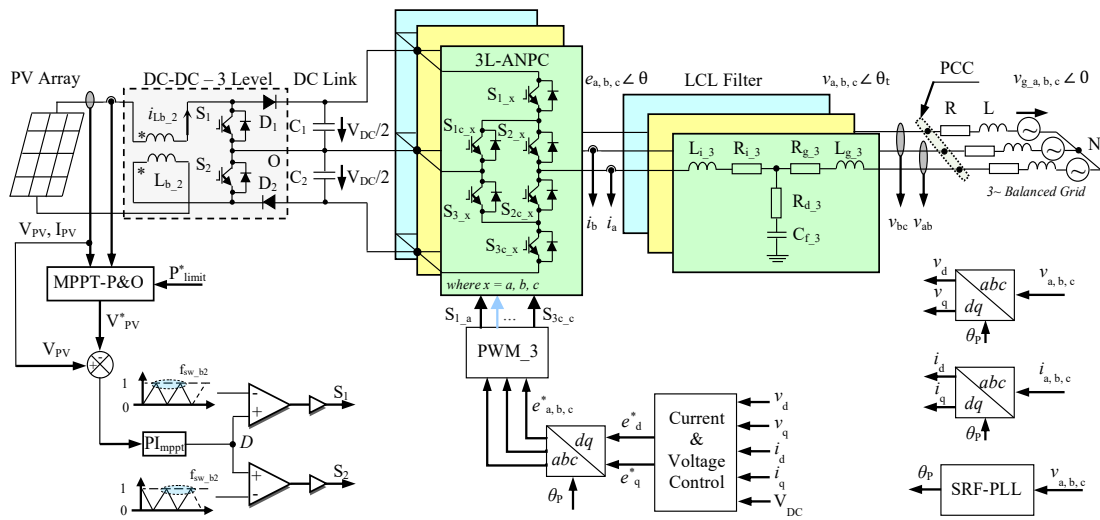


Fig. 6 – Grid-connected system based on 3L-ANPC and 3L dc-dc boost topology.

As in the previous case, the harmonic content at the inverter output differs, therefore a new LCL filter is needed. The 3L-ANPC structure has six active switches on each bridge arm, the two additional switches replacing the clamp diodes in the NPC structure. Functionally, the switches support half of the dc supply voltage, but due to the structure of this inverter, the thermal stress at the switches is more balanced, unlike the NPC topology where this balancing does not exist.

The control of the 3L-ANPC inverter is also based on the optimal SPWM technique [7], which allows doubling the apparent switching frequency for output voltages. The frequency of the two carrier signals was considered, as in the previous cases,  $f_{sw} = 5$  kHz. Due to the doubling of the apparent switching frequency, the harmonics on the output side of the inverter will be placed around frequencies of 10 kHz and multiples. Thus, the passive filter was optimized. Optimization that will translate into cost reduction because the amount of copper in the coils is reduced. The new relationship for calculating the filter inductance on the  $L_{i,3}$  inverter side is as follows:

$$L_{i,3} \geq \frac{V_{DC}}{16 \cdot f_{sw} \cdot \Delta i_{max}}, \quad (15)$$

resulting in a value of  $L_{i,3} = 2.1$  mH, a value twice as low as the 3L-NPC inverter, while the values of the maximum current ripple and frequency are equal to those of the previous case.

Following the same reasoning as in the previous cases, the following parameters were obtained: filter capacitance  $C_{f,3} = 5$   $\mu$ F, a factor  $r_3 = 0.67$ , so  $L_{g,3} = 1.4$  mH, and an attenuation resistance  $R_{d,3} = 5.5$   $\Omega$ . The parameters of the current regulators,  $PI_{d,3}$  and  $PI_{q,3}$ , were calculated so that the stability conditions were met.

#### 4. RESULTS AND ANALYSIS

The three cases of grid-connected PV systems presented were modeled and simulated. To test these configurations, a light intensity profile with a stepped variation was considered. Following the simulations performed, on the output side of the LCL filter, approximately the same current and voltage waveforms were obtained, small

differences could be neglected. For this reason, only a set of results for case 3L-ANPC is presented.

Therefore, the three-phase voltages system at the output of the LCL filter is the one in Fig. 7.a, where regardless of the power level injected into the grid ( $P$ ), the voltage amplitude is the same. The mode of variation of the three-phase currents system is imposed by the power level supplied by the PV array (Fig. 7.b). Since the voltage does not change, the current will follow a profile like that of the luminous intensity. This profile is imposed by the reference current  $i_d^*$ . Another important remark is that regardless of the power level  $P$  (Fig. 7.c), the voltage in the dc-link remains almost constant (Fig. 7.d).

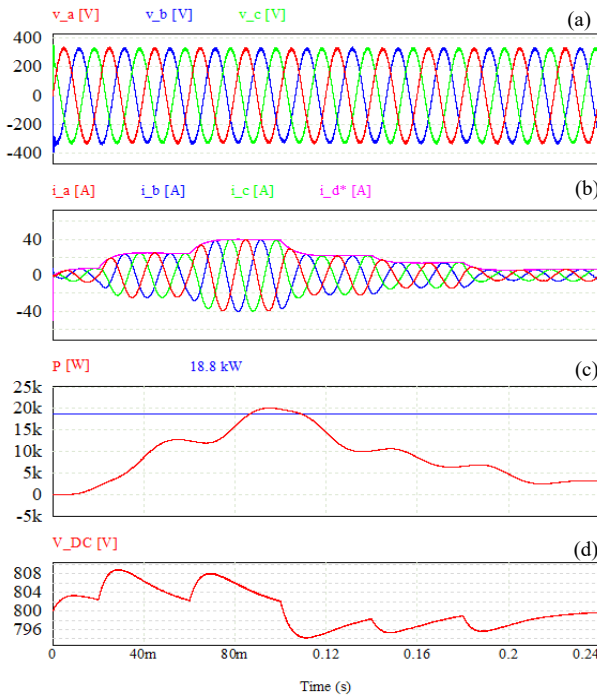


Fig. 7 – Simulate results for the grid-connected system using 3L-ANPC.

For the PV 3L-ANPC system, a power limitation has been introduced for the PV array. Thus, the  $P_{limit}^*$  was set to 8kW, as shown in Fig. 8.a. Thus, the power injected ( $P$ ) by the inverter into the grid stabilizes at this level after a short overshoot sequence (Fig. 8.b). The power limitation can come from a dispatcher that monitors grid parameters. If there is not enough consumption, then it will impose a greater limitation so that the network is not disturbed. As was mentioned throughout the material, all the limiting part is implemented at the MPPT level. The dc-dc stage brings the power from the panels to the dc-link, and the inverter, through the direct current loop, takes the power from the dc-link and injects it into the grid.

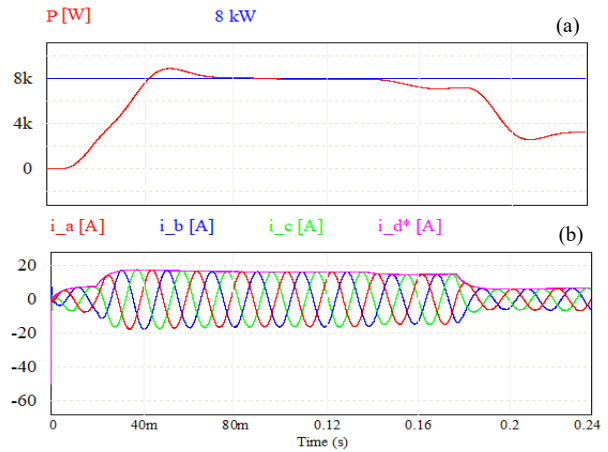


Fig. 8 – Simulate results for 3L-ANPC system with power limit.

## 5. CONCLUSIONS

The characteristics of three systems suitable for grid connection of solar panels have been highlighted throughout the paper. If a simple application is desired, both in terms of the conversion structures and the control part, then the classical PV system can be chosen.

The 3L structures used in this work have the advantage that they offer a lower harmonic content on the output side so that the filter inductance values could be reduced. The power devices support only half of the supply voltage, so their cost will be lower than the first case. Also, in the 3L dc-dc boost converter, the inductance could be reduced by half, as well as the switching frequency value, obtaining an effect identical to the first case.

Cases studied with multilevel converters are suitable both for applications with an installed power of several tens of kilowatts and for large powers. As the installed power increases, multilevel structures are preferred because the power losses are lower compared to the 2L case, and the voltage waveform on the output side is closer to a sine. The drawback of 3L systems is the complexity of the control part. However, the control strategy has made it possible to achieve a notable optimization in the last case of the studied PV system using 3L-ANPC.

Received on 28 April 2022.

## REFERENCES

1. Y. Yang, K. Kim, F. Blaabjerg, A. Sangwongwanich, *Advances in grid-connected photovoltaic power conversion systems*, 1 ed. Duxford: Woodhead Publishing, 2018. pp. 15-43.
2. Q. Peng, J. Fang, Y. Yang, F. Blaabjerg, *A universal model for grid-connected converters reflecting power-internal voltage characteristics*, IEEE 4th Southern Power Electronics Conference, pp. 1-7 (2018).
3. Y. Huang, X. Zhai, J. Hu, D. Liu, C. Lin, *Modeling and stability analysis of vsc internal voltage in dc-link voltage control timescale*, IEEE Journal of Emerging and Selected Topics in Power Electronics, 6, 1, pp. 16-28 (2018).
4. Y. Huang, X. Yuan, J. Hu, P. Zhou, *Modeling of VSC connected to weak grid for stability analysis of dc-link voltage control*, IEEE Journal of Emerging and Selected Topics in Power Electronics, 3, 4, pp. 1193-1204 (2015).
5. A. Sangwongwanich, Y. Yang, F. Blaabjerg, *Development of flexible active power control strategies for grid-connected photovoltaic inverters by modifying MPPT algorithms*, IEEE 3rd International Future Energy Electronics Conference and ECCE Asia, pp. 87-92 (2017).

6. S. Kouro, J.I. Leon, D. Vinnikov, L.G. Franquelo, *Grid-Connected Photovoltaic Systems: An Overview of Recent Research and Emerging PV Converter Technology*, IEEE Industrial Electronics Magazine, **9**, 1, pp. 47-61 (2015).
7. D. Floricău, E. Floricău, M. Dumitrescu, *Natural doubling of the apparent switching frequency using three-level ANPC converter*, 2008 International School on Nonsinusoidal Currents and Compensation, pp. 1-6 (2008).
8. D. Floricău, D. Olaru, E. Floricău, I. Popa, *Loss balancing in three-level active-neutral-point-clamped converter*, Rev. Roum. Sci. Techn. – Électrotechn. Et Énerg., **54**, 3, pp. 281–290 (2009).
9. A.K. Podder, N.K. Roy, H.R. Pota, *MPPT methods for solar PV systems: a critical review based on tracking nature*, IET Renew. Power Gener., **13**, 10, pp. 1615–1632 (2019).
10. A. Amine, A. Massoum, M. Chadli, *Comparison study of two tracking methods for photovoltaic systems*, Rev. Roum. Sci. Techn. – Électrotechn. Et Énerg., **60**, 2, p. 205–214 (2015).
11. F. Blaabjerg, R. Teodorescu, M. Liserre, A.V. Timbus, *Overview of control and grid synchronization for distributed power generation systems*, IEEE Trans. on Industrial Electronics, **53**, 5, pp. 1398-1409 (2016).
12. Q. Peng, A. Sangwongwanich, Y. Yang, F. Blaabjerg, *Grid-friendly power control for smart photovoltaic systems*, Solar Energy, **210**, pp. 115-127 (2020).
13. A. Timbus, M. Liserre, R. Teodorescu, F. Blaabjerg, *Synchronization methods for three-phase distributed power generation systems – An overview and evaluation*, IEEE 36th Power Electronics Specialists Conference, pp. 2474-2481 (2005).
14. P. Rodriguez, R. Teodorescu, I. Candela, A. V. Timbus, M. Liserre, F. Blaabjerg, *New positive-sequence voltage detector for grid synchronization of power converters under faulty grid conditions*, in Proc. IEEE PESC, pp. 1–7 (2006).
15. P. Rodriguez, J. Pou, J. Bergas, J.I. Candela, R.P. Burgos, D. Boroyevich, *Decoupled double synchronous reference frame PLL for power converters control*, IEEE Trans. on Power Electronics, **22**, 2, pp. 584-592 (2007).
16. J. Y. Lee, Y. P. Cho, H. S. Kim, J. H. Jung, *Design methodology of passive damped LCL filter using current controller for grid-connected three-phase voltage-source inverters*, J. of Power Electronics, **18**, 4, pp. 1178-1189 (2018).
17. A. Julean et al., *Active damping of LCL filter resonance in grid-connected applications*, Master Thesis, Aalborg University (2009).
18. S.V. Araujo, A. Engler, B. Sahan, F.L. M. Antunes, *LCL filter design for grid-connected NPC inverters in offshore wind turbines*, 7th International Conference on Power Electronics, pp. 1133-1138 (2007).
19. D. Floricău, T. Tudorache, L. Kreindler, *New boost-type PFC MF-Vienna PWM rectifiers with multiplied switching frequency*, Advances in Electrical and Computer Engineering, **15**, 4, pp. 81-86 (2015).
20. M. Fliitti, M-K. Fellah, M. Khatir, S-A. Zidi, M-F. Benkhoris, *Control of back-to-back voltage source converter*, Rev. Roum. Sci. Techn. – Électrotechn. Et Énerg., **57**, 3, pp. 259–268 (2012).
21. M. Liserre, F. Blaabjerg, S. Hansen, *Design and control of an LCL-filter-based three-phase active rectifier*, IEEE Trans. on Industry Applications, **41**, 5, pp. 1281-1291 (2005).
22. H. Chen, W. Lin, *MPPT and voltage balancing control with sensing only inductor current for photovoltaic-fed, three-level, boost-type converters*, IEEE Trans. on Power Electronics, **29**, 1, pp. 29-35 (2014).